Chapter 3

MODELS OF GAP DETECTION IN ACOUSTIC HEARING

1 INTRODUCTION

Gap detection has often been used as a measure of temporal resolution in the auditory system, e.g. Penner (1977), Divenyi and Danner (1977), Fitzgibbons (1984), Formby and Forrest (1991). The gap detection task has traditionally been within-channel (i.e. gap markers were the same). Across-channel gap detection has been used in acoustic stimulation (Phillips et al., 1997) to investigate how temporal gaps between spectrally different sounds are detected, a situation that is typical in everyday speech understanding tasks. It has been hypothesized that across-channel gap detection thresholds reflect the extent of neural activation (Hanekom and Shannon, 1998; chapter 2). In both the acoustic and electrical stimulation cases, it has been found that gap thresholds increase as the gap markers are separated in frequency (Divenyi and Danner, 1977; Divenyi and Sachs, 1978; Phillips et al., 1997; Formby and Forrest, 1991; Formby, Sherlock, and Forrest, 1996) or presented on two electrode pairs with increasing spacing (Hanekom and Shannon, 1998). Examples of the resulting U-shaped gap detection "tuning curves" have been given in chapter 2.

A model of gap detection in acoustic hearing is created in this chapter, with the primary objective of investigating which underlying factors bring about the U-shaped gap detection curves found in across-channel gap detection tasks.

1.1 Models of gap detection in acoustic auditory stimulation

Previous models of auditory duration discrimination or gap detection have been presented by Creelman (1962), Formby, Sherlock, and Forrest (1996), Forrest and Formby (1996), and Heinz, Goldstein, and Formby (1996). Creelman (1962) modelled duration discrimination of

brief signals in a signal detection theoretical context. He hypothesized that an internal counter counted the number of spikes elicited by a brief signal to measure the signal duration. The spike train was assumed to be Poissonian, so that noise was present in the duration measurement, but the signal onset and offset were assumed to be known exactly. Divenyi and Danner (1977) expanded this model to include the effects of noise in the determination of the signal offset and onset in gap discrimination. These models cannot explain the U-shaped curves found in across-channel gap detection.

In a series of articles, Formby and co-workers (Formby et al., 1996; Forest and Formby, 1996; Heinz et al., 1996) described models for gap detection with sinusoidal markers that differed in frequency. They ascribed the increased gap thresholds in across-channel gap detection to peripheral filtering. They noted that listeners may enhance gap thresholds when permitted to improve signal-to-noise ratio by shifting the auditory filter centre frequency to midway between the two marker frequencies. In essence, their single channel model (Forrest and Formby, 1996) had a single auditory filter stage (including nonlinear compression to model stimulus transduction at the hair cell) that bandpass-filtered the marker frequencies. This auditory filter was centred between the two marker frequencies to optimize performance on the gap detection task. The simulation used the same 2IFC procedure as used with listeners. The filter outputs in the two intervals of the 2IFC procedure were compared and the interval with the largest ratio of maximum to minimum output (the max-min statistic) was chosen as the interval containing the gap. Simulated gap thresholds could be obtained by taking the average of several model runs. The model generated results similar to those of human listeners in a gap detection task, except that the asymptotic thresholds for large marker frequency separations could not be reproduced.

The multi-channel model of these authors (Heinz, Goldstein, and Formby, 1996) is similar to the single-channel model, but used multiple bandpass filters and calculated the max-min ratio for each channel. Each channel then decided which of the two intervals in the 2IFC procedure contained the gap, and the final decision was base on a majority vote. Only channels within a decision region centred between the two marker frequencies were included in the decision. The

model generated results similar to those of human listeners in a gap detection task.

1.2 Extension of previous models

The model described in this chapter extends the work of Formby and co-workers in two respects:

(1) Closed form equations are obtained for gap discrimination and gap detection thresholds. This makes the model easy to interpret and allows effortless investigation of the effects of model parameters.

(2) The model is developed to be more detailed and closer to the underlying neurophysiology, by using spike trains and spike train statistics to derive equations for gap thresholds. This is important, as spike train statistics are dramatically different in electrical stimulation of the auditory nerve. The models of Formby and co-workers cannot be used for prediction of gap thresholds in electric hearing.

Consequently, by using the statistics of the spike train (rather than the max-min statistic based on analogue waveforms as in Formby), modelling what happens in both electrical stimulation and acoustic stimulation is possible. The basic principle used in the model in this and the next chapter is that neural channels stimulated by gap markers that are more closely spaced (in frequency or in physical electrode position), result in an easier gap detection task so that gap thresholds decrease. Following the arguments of Formby and co-workers, it is assumed that the auditory system places a filter between the two areas stimulated by the two markers. The exact nature of this filter is unimportant. This may be an "attentional filter" as suggested by Divenyi and Danner (1977) and Phillips et al. (1997). The current model makes this notion explicit. As the markers move apart, the task of the gap detector becomes more difficult, because the difference in spike rate during the marker and within the gap becomes smaller.

Conceptually, the model presented in this chapter incorporates the following ideas. Two factors limit measurement of the duration of a temporal gap. Uncertainty exists about the times at which the edges of the gap occur, and when the edges are known (or have been estimated)

there is noise in the actual measurement of the duration of the gap. The origin of this noise is the Poissonian nature of the spike trains in the central auditory nervous system.

1.3 Objectives of this chapter

A model of gap detection in acoustic hearing is created in this chapter, with the objective of investigating which underlying factors bring about the U-shaped gap detection curves found in across-channel gap detection tasks. This model extends previous models as described above. As it is believed that the same underlying mechanisms operate in acoustic and electrical gap detection, the intention is to create a model that can also be expanded for the electrical gap detection situation (see chapter 4).

2 A MODEL FOR GAP DETECTION IN ACOUSTIC HEARING

2.1 Assumptions about the acoustically evoked spike train

At the auditory periphery, an estimate of when the edges of the gap occur may be influenced by three different situations. First, in acoustic stimulation, spike trains are random and Poisson-like for high frequencies (above 5 kHz). In this case, the positions of the edges of a gap will be the most difficult to estimate, and gap thresholds may have been expected to be the largest of the three cases. Second, for low frequencies (acoustic stimulation below 5000 Hz), spike trains are phase-locked to the cycles of the stimulus (e.g., Johnson (1980)). This may have been expected to improve the ability to judge the edges of the gap accurately. However, Shailer and Moore (1983) showed that a close correspondence exists between the auditory filter bandwidth and gap detection thresholds at low frequencies. Also, gap thresholds decrease for increasing frequencies (Fitzgibbons, 1983; Fitzgibbons, 1984). This effect has been ascribed to the decreasing auditory filter bandwidth at lower frequencies, which presumably leads to more ringing in these narrower auditory filters, and to inherent fluctuations in narrowband noise (Shailer and Moore, 1983; Shailer and Moore, 1987). The rate of fluctuation is determined

approximately by the reciprocal of the bandwidth of the filter. Smaller bandwidth results in slower fluctuations, that may be confused with the gap.

Third, for electrical stimulation, spikes are tightly phase-locked, especially to pulsatile stimulus waveforms (Javel, 1990). The only limitation in the correct judgement of the positions of gap edges is the small jitter in spike positions relative to a preferred latency. If gap detection was based on temporal information only, gap detection might have been expected to be more acute than in normal hearing, but results show that gap detection thresholds in cochlear implantees are similar to those measured in normal-hearing listeners (Shannon, 1989).

These observations suggest that temporal phase-locking does not play a major role in determining gap thresholds, but that spatial mechanisms (i.e. peripheral filtering) may play a more important role, consistent with the models of Formby and co-workers as cited above. Of course, peripheral filtering does not play a role in cochlear electrical stimulation, but the current distribution from the site of an electrode may play a role similar to an auditory filter. This idea is expanded in chapter 4.

Based on the foregoing observations, the use of Poisson processes in the gap detection model to model spike trains seems justifiable, especially for acoustic stimulation. Assuming that spike trains are Poisson processes simplifies the mathematical analysis.

2.2 Nerve fibre model

The nerve fibre model used in the acoustic gap detection models is described here. The gap detection model is based primarily on the rate response profile (called the λ-profile in this text, where λ is the average rate parameter in a Poisson process that describes neural spike train). The nerve fibre model has a significant influence on the λ-profile, which in turn influences the size of $\Delta\lambda$ when the gap marker frequencies are separated. $\Delta\lambda$ is the difference in spike rates during the gap and markers. The larger this rate difference, the more detectable the transition from marker to gap or gap to marker becomes.

2.2.1 Nature of the nerve fibre model

The fibre model described is not a biology-based model, but rather a black box model that incorporates the major spike train characteristics that are important in audition. The well-known Hodgkin-Huxley model, e.g. Kistler, Gerstner, and van Hemmen (1997), is an example of what is termed here a biology-based model. It incorporates the nerve fibre cell membrane dynamics to predict firing characteristics in response to stimuli. Neither the Hodgkin-Huxley model, nor the current model has any statistical characteristics. They always fire when threshold is reached, unlike biological models that incorporate sources of noise, e.g. Lecar and Nossal (1971).

The nerve fibre model used in this chapter is an average rate model, meaning that it models the average spike count characteristics, but not the instantaneous spike characteristics. For example, the fibre model does not incorporate phase-locking of spike trains to a preferred stimulus phase (see chapter 5). The nerve fibre model can be used for calculating λ-profiles and predicting average firing rates. Finally, the model is based on pure-tone stimulus data. The input to the fibre model is the frequency f and amplitude A of a pure tone stimulus. The output is the average firing rate at different locations in the cochlea.

2.2.2 Nerve fibre model equations

The nerve fibre model builds on a model by Colburn (1973). The model is straightforward and simple to interpret. The average rate for fibre *m* for a pure tone stimulus of frequency *f* is

$$\overline{r_m} = SR + MR \cdot g(A) \cdot H_m(f) . \tag{3.1}$$

In this equation, SR is the spontaneous rate of the fibre, MR is the maximum rate, A is the stimulus intensity in dB SPL, g(A) is a function that characterizes spike rate as a function of intensity (rate-intensity curve), and $H_m(f)$ is a tuning parameter (explained below). The function g(A) is

$$g(A) = \frac{1}{2}\left(1 + Erf\left(\frac{A - A_{thr}(m)}{\sqrt{2}\sigma}\right)\right) . \tag{3.2}$$

This is an integrated Gaussian that provides an s-shaped curve that can be fitted to typical rate-intensity data. The parameter σ controls the slope of the curve. $A_{thr}(m)$ is the threshold of fibre m in dB SPL. By definition, threshold is reached when the spike rate increases by 10% from SR. Thresholds of fibres excited by the stimulus (of frequency *f*) differ as fibres may be stimulated at a frequency different from their CF. Fibres stimulated at their CF have the lowest threshold, and the threshold increases as fibres are stimulated with frequencies increasingly different from CF. This is described by the tuning function $H_m(f)$. Thus $A_{thr}(m)$ in equation 3.2 is

$$A_{thr}(m) = A_{thr,CF} + A_{off} + 20\log H_m(f)\,. \tag{3.3}$$

$A_{thr}(m)$ is the threshold of a fibre at a specific stimulus frequency *f*, when the best frequency for that fibre is CF. $A_{thr,CF}$ is the threshold at CF in dB SPL. Typical values for $A_{thr,CF}$ are 0 to 30 dB SPL (as determined in cat by Shofner and Sachs, 1986). g(A) takes on values between 0 and 1 and is centred on A_{thr}, unless the offset parameter A_{off} is used, i.e., at A_{thr} there is already a 50% increase in spike rate. The offset parameter A_{off} is used to ensure that the spike rate has increased by 10% at A_{thr}.

For a fixed value, the parameter σ results in a fixed slope for the rate-intensity curve. However, data show that the slope changes for stimulus frequency *f* more distant from CF for frequencies above CF (Evans, 1975; also see Javel and Viemeister, 2000). A model for σ is then

$$\begin{aligned} &\text{for } f \le f_m: \quad \sigma = \sigma_0\,, \\ &\text{for } f > f_m: \quad \sigma = \sigma_0 + \left(\frac{f - f_m}{f_m}\right) \cdot k\,, \end{aligned} \tag{3.4}$$

where f_m is the CF of fibre *m*. Parameter *k* changes the slope as a function of $|f-f_m|$. To fit the data in Colburn (1973), σ_0=5 is used, while σ_0=6 and *k*=20 provides a reasonable fit to the data in Evans (1975).

The tuning function $H_m(f)$ in equations 3.1 and 3.3 characterizes the threshold of a fibre with

best frequency CF when the acoustic stimulus frequency is varied. Thus, it is (the inverse of) a normalized frequency tuning curve (maximum tuning is 1), so that 20 log H_m gives an approximation to the tuning curve, but has threshold at 0 dB. The actual threshold at CF is then specified explicitly in equation 3.3 as $A_{thr,CF}$. $H_m(f)$ is given by

$$\begin{aligned} H_m(f) &= \left(\frac{f}{f_m}\right)^{\alpha} \quad for\ f \le f_m \\ &= \left(\frac{f_m}{f}\right)^{2\alpha} \quad for\ f > f_m\ . \end{aligned} \tag{3.5}$$

The parameter α controls the rolloff of the tuning curve, and is given by

$$\begin{aligned} \alpha &= \alpha_0 \quad for\ f_m \le 800\ Hz \\ &= \alpha_0 \cdot \frac{f_m}{800} \quad for\ f_m > 800\ Hz\ . \end{aligned} \tag{3.6}$$

α_0 =4 provides a good fit to the AN data. Note that the rolloff becomes sharper at higher frequencies. These last two are the same equations as given in Colburn (1973). The tip part of the data is fitted well, but not the tail. For the current model, the tail is ignored.

The set of equations from 3.1 to 3.6 define the auditory nerve fibre model.

2.3 Cramer-Rao Lower Bound for the Poisson change-point problem

The objective of this section is to derive a simple equation for the gap threshold as a function of the difference in spike rates elicited by the pre-gap and post-gap markers. The Poissonian nature of the neural spike trains complicates the detection of the edges of a gap, as it makes a change in spike rate difficult to detect. The Cramer-Rao Lower Bound (CRLB) for the detection of the gap edges is derived for this problem. The CRLB gives the variance in the estimate of a (classical) optimal estimator.

The problem is to calculate the CRLB for the time of a step change in the rate of a Poisson

process. It is natural to suspect that the accuracy with which the change-point may be found depends on the difference in rates of the Poisson process before and after the step change, as well as the time that the detector has to observe the non-homogeneous Poisson process. The rate of change of the rate function (i.e. whether it is a step function or a ramp) should also influence the accuracy of the change-point detection.

As far as is known, the CRLB for the Poisson change-point problem has not been addressed in literature. Much literature exists on solving the change-point problem for Poisson processes (e.g.Bremaud (1981), Karr (1986), Davis (1976), Raftery and Akman (1986), West and Ogden (1994), Gal'chuk and Rozovskii (1971)), but the objective of all of these authors was to find an algorithm to detect the change-point in a given Poisson process, rather than addressing the question of how accurately this could be done.

A parallel problem is that of determining the change-point of a signal in Gaussian noise that has a step change in amplitude. The task in this case is to estimate the time of step change by observing the signal plus noise. Samples are taken at regular intervals, whereas in the Poisson problem no sampling is done, but the discrete or continuous point process is observed. This signal in Gaussian noise problem is solved in e.g. McDonough and Whalen (1995). It may be expected that the change point detection accuracy is dependent on the variance of the Gaussian noise, as well as the differences in signal amplitude before and after the step, and also the time that the detector has for observation before and after the step. The CRLB on this estimate has been calculated in Reza and Doroodchi (1996).

The CRLB for signals in Gaussian noise may then be used as an estimate of the bound for the Poisson problem. For a Poisson process, the average rate λ equals the variance, so a signal that jumps in amplitude from A_1 to A_2 at time τ, can be equated to a Poisson process that has a jump in rate from $A_1=\lambda_1$ to $A_2=\lambda_2$. The variance of the Gaussian noise is λ_1 before the jump and λ_2 after the jump. This argument redefines the Poisson problem as a signal in Gaussian noise problem.

To calculate the CRLB, a differentiable function is required to characterize the jump in rate of the Poisson process. A sigmoidal function may be used to model the change-point, instead of a step change. For a jump from average rate λ_1 to average rate λ_2 at a change-point time τ, the rate of the Poisson process is given by equation 3.7,

$$\lambda_t(\tau) = \lambda_1 + \frac{(\lambda_2 - \lambda_1)}{1 + e^{-\alpha(t-\tau)}} = \frac{\lambda_2 + \lambda_1 e^{-\alpha(t-\tau)}}{1 + e^{-\alpha(t-\tau)}}, \tag{3.7}$$

where α determines the rate of change from λ_1 to λ_2. As shown in equation 3.26, α is inversely proportional to Δt, where Δt is the duration of a transition from λ_1 to λ_2. Physical factors determine Δt, as the transition between marker and gap cannot occur instantaneously. The data of Zhang, Salvi, and Saunders (1990) show that spike rate decays exponentially after the offset of a gap marker with time constants in the order of 1 ms. Westerman and Smith (1984) measured minimum decay time constants of 1 ms in auditory nerve fibres. As shown below equation 3.6, this implies values in the order of α=4000.

The CRLB is $1/F(\theta)$ with $F(\theta)$ the Fisher information and θ a parameter. Snyder (1975) derived a general form for the Fisher information for Poisson processes,

$$F(\theta) = \int_{t_0}^{T} \left(\lambda_t(\theta)\right)^{-1} \left(\frac{\partial \lambda_t(\theta)}{\partial \theta}\right)^2 dt\,. \tag{3.8}$$

$F(\theta)$ is a function of the *intensity* λ_t of the Poisson process only. $[t_0, T]$ is the period over which the CRLB is required. For the signal model in equation 3.7, the Fisher information, parameterized by τ, may be rewritten as

$$F(\tau) = \int_{0}^{T} \left(\lambda_t(\tau)\right)^{-1} \left(\frac{\partial \lambda_t(\tau)}{\partial \tau}\right)^2 dt\,. \tag{3.9}$$

It follows from equation 3.7 that

$$\frac{\partial \lambda_t(\tau)}{\partial \tau} = \frac{\alpha e^{-\alpha(t-\tau)}(\lambda_1 - \lambda_2)}{(1 + e^{-\alpha(t-\tau)})^2}. \tag{3.10}$$

Accordingly, the Fisher information is

$$F(\tau) = \int_0^T \frac{\alpha^2 e^{-2\alpha(t-\tau)}(\lambda_1 - \lambda_2)^2}{(1 + e^{-\alpha(t-\tau)})^3(\lambda_1 e^{-\alpha(t-\tau)} + \lambda_2)} dt. \tag{3.11}$$

The integral in equation 3.11 has a solution in closed form, but this solution is a rather complicated expression that does not provide insight into the effect of the different variables (λ_1, λ_2 and α) on the accuracy with which τ can be estimated. Therefore, equation 3.11 is solved numerically. The CRLB gives the variance in the estimate of τ and is calculated as the inverse of equation 3.11.

One approach for obtaining a closed-form expression for the CRLB in terms of λ_1 and λ_2, is to approximate the Poisson process by a Gaussian process as explained above. An equivalence between the two processes exists when the Poisson process is interpreted as a discrete Poisson process. The discrete Poisson process with intensity λ_1 has an average of $\lambda_1 T$ points in a time interval T. The variance in the number of points in T is also $\lambda_1 T$. Accordingly, the discrete Poisson process is equivalent to a Gaussian process with a sampling period of T seconds, average $\lambda_1 T$ and variance $\lambda_1 T$. The problem of estimating the change-point in a Gaussian process has been solved by Reza and Doroodchi (1996). Their model is similar to equation 3.7, but they discretized the problem. In their formulation, the objective is to estimate the discrete sampling interval n_0 in which the change-point occurs. The solution is

$$CRLB = \frac{8}{(d')^2 \alpha T} \cdot \left(\sum_{n=0}^{N-1} J_k\right)^{-1} = var(\hat{n}_0), \tag{3.12}$$

where T is the sampling interval and N samples are observed. α is the rate of change parameter as before, d' is a parameter that measures the distance between the two pdfs, and J_k is defined

below. If the average value of the two Gaussian pdfs were m_1 and m_2 and the two distributions had the same variance σ,

$$d' = \frac{m_1 - m_2}{\sigma}. \tag{3.13}$$

d' may be interpreted as a signal-to-noise ratio. For $\sigma_1 \neq \sigma_2$ the average $\sigma^2 = (\sigma_1^2 + \sigma_2^2)/2$ is used. Substituting $\lambda_1 T$ for m_1 and $\lambda_2 T$ for m_2, $\lambda_1 T$ for σ_1^2 and $\lambda_2 T$ for σ_2^2, d' is found as

$$(d')^2 = \frac{2T(\lambda_1 - \lambda_2)^2}{\lambda_1 + \lambda_2}. \tag{3.14}$$

J_k in equation 3.12 is given by Reza and Doroodchi as

$$J_k = \tanh a_k - \tanh b_k - \frac{1}{3}(\tanh^3 a_k - \tanh^3 b_k), \tag{3.15}$$

with $a_k = \frac{\alpha T}{2}(k - n_0)$ and $b_k = a_k - \frac{\alpha T}{2}$.

When equation 3.14 is substituted into equation 3.12, a closed-form expression for the CRLB in terms of λ_1 and λ_2 is obtained as

$$var(\hat{n}_0) \geq \frac{4(\lambda_1 + \lambda_2)}{\alpha T^2(\lambda_2 - \lambda_1)^2} \cdot \left(\sum_{n=0}^{N-1} J_k\right)^{-1}. \tag{3.16}$$

The solution in equation 3.16 is an approximation to the actual CRLB that can be calculated from equation 3.11, but as figure 3.1 shows, the approximation is quite acceptable. The variance in equation 3.16 is in number of sampling intervals, so that $var(\hat{\tau}) = T^2 \cdot var(\hat{n}_0)$.

If multiple observations of the same signal is available, it is generally true that the signal-to-noise ratio (SNR) for estimating the signal improves. Thus if the same change in rate of the Poisson process is observed in M simultaneous but independent Poisson processes, the signal-to-noise ratio (SNR) improves as indicated in equation 3.17,

$$SNR_M = \sum_{i=1}^{M} SNR_i. \tag{3.17}$$

Generally, SNR_i will not be the same in different fibres that convey information about the same signal, but in this model the M fibres are within the same critical band (as explained in section 2.4) so that the SNR_i are of comparable magnitudes in these channels. To simplify calculations, it is assumed that the SNR_i are identical in the M channels, so that $SNR_M = M \cdot SNR$. For the CRLB calculation this implies that the minimum variance in the estimate of τ is obtained when the SNR is the signal-to-noise ratio of the channel with the largest difference between λ_1 and λ_2 (if it is assumed that λ_1 and λ_2 are not equal on all M channels).

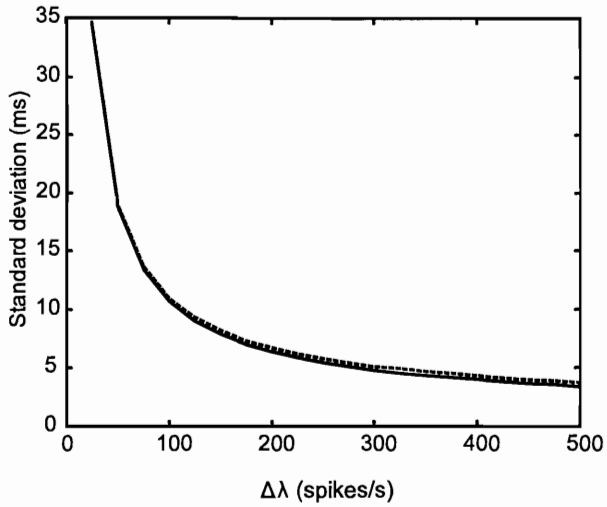

Figure 3.1

This figure shows the standard deviation in the estimate of the position of a gap edge, calculated from equation 3.11 (solid line) and equation 3.16 (dashes). The values calculated from equation 3.16 were multiplied by T to obtain the standard deviation in ms.

For the detection of a gap, λ_1 may be the rate during the marker, while λ_2 may be the rate during the gap. For within-channel gap detection, the task is to detect the change in rate, and not to estimate the time of change. Thus, the probability P of detection as a function of $\Delta\lambda$,

where $\Delta\lambda = |\lambda_2 - \lambda_1|$, is required. The gap threshold is assumed to be at P = 0.76. For across-channel gap detection, the task is to discriminate between gap lengths in the two intervals.

The final equation for the variance in the estimate of τ is therefore

$$var(\hat{\tau}) = \frac{T^2 \cdot 4(\lambda_1 + \lambda_2)}{\alpha T^2(\lambda_2 - \lambda_1)^2} \cdot \frac{1}{\sum_{n=0}^{N-1} J_k} \cdot \frac{1}{M}$$
$$= \frac{4(\lambda_1 + \lambda_2)}{\alpha(\lambda_2 - \lambda_1)^2} \cdot \frac{1}{\sum_{n=0}^{N-1} J_k} \cdot \frac{1}{M}. \qquad (3.18)$$

The summation in equation 3.18 does not lend itself to physical interpretation. Arriving at an even simpler form of equation 3.18 by the following derivation is possible. Suppose the task is to estimate the time of change τ of the average value of a Gaussian process (figure 3.2), from a value A_1 to a value A_2. The Gaussian process has a standard deviation σ_y. Let the change take place within Δt seconds. The task is to estimate the time of change τ at the centre of the transition. This task is the same as estimating the time at which the Gaussian process has an average value exactly halfway between A_1 and A_2. Because of the Gaussian noise in measurement of σ_y, there is noise in the estimate of τ. Thus, the Gaussian variable on the y-axis is transformed to another Gaussian variable on the t-axis. The average value of this Gaussian is τ, while the standard deviation is σ_t. It can easily be shown that

$$\sigma_t = \frac{\Delta t}{A_2 - A_1}\sigma_y. \qquad (3.19)$$

This is the standard deviation in the estimate of τ when one sample is taken at the time when the average value of the Gaussian is $(A_1+A_2)/2$. It follows for M samples that

$$var(\hat{\tau}) = \Delta t^2 \cdot \frac{\sigma_y^2}{(A_2 - A_1)^2} \cdot \frac{1}{M} = \frac{\Delta t^2}{SNR} \cdot \frac{1}{M}. \tag{3.20}$$

If, as before, the Poisson process is discretized, SNR may be substituted by equation 3.14 to obtain

$$var(\hat{\tau}) = \frac{\Delta t^2 \cdot (\lambda_1 + \lambda_2)}{2T(\lambda_2 - \lambda_1)^2} \cdot \frac{1}{M}. \tag{3.21}$$

Therefore,

$$std\ dev(\tau) = \sqrt{\frac{\Delta t^2(\lambda_1 + \lambda_2)}{2T(\lambda_2 - \lambda_1)^2} \cdot \frac{1}{M}}. \tag{3.22}$$

The equivalence between equations 3.18 and 3.22 is clear. Note that while equation 3.18 gives the minimum standard deviation predicted by the CRLB, equation 3.22 is the actual standard deviation of an estimate formed as described above. For $\alpha >> 1$, (for rapid transitions) the summation term in equation 3.18 saturates at a value of 4/3. It will be shown below that α will always be large in these calculations. Equation 3.18 simplifies to

$$var(\hat{\tau}) = \frac{3(\lambda_1 + \lambda_2)}{\alpha(\lambda_2 - \lambda_1)^2} \cdot \frac{1}{M}. \tag{3.23}$$

Comparison of equation 3.21 and equation 3.23 suggests that an equivalent α may be found for a transition duration of Δt seconds. If the slope of a sigmoidal function at $t=\tau$ in equation 3.7 is equated to the slope of the transition in figure 3.2, α can be solved for in terms of Δt. The slope is

$$\frac{\partial \lambda_t(\tau)}{\partial t} = \frac{\alpha (A_2 - A_1) e^{-\alpha (t-\tau)}}{(1 + e^{-\alpha (t-\tau)})^2} . \tag{3.24}$$

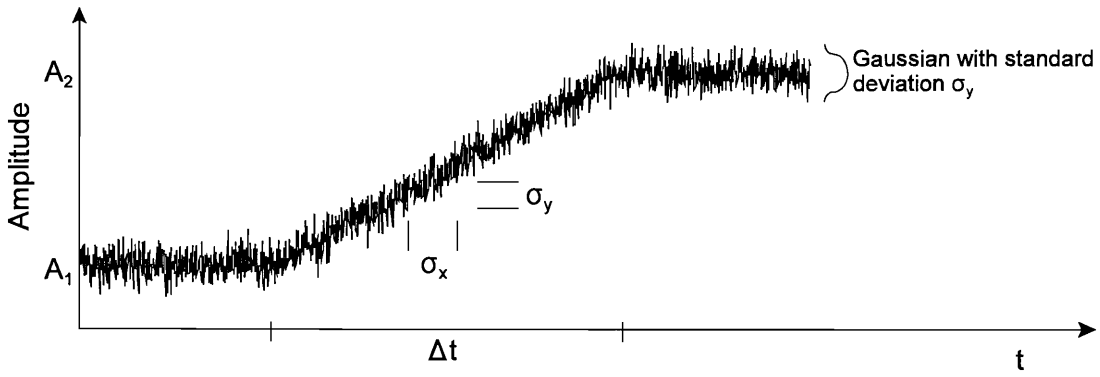

Figure 3.2

The Poisson change-point problem is re-interpreted as a Gaussian change-point problem, which is shown in this figure. The transition from average value A_1 to average value A_2 takes Δt seconds.

Replacing t with τ and equating this with the slope of the transition in figure 3.2,

$$\frac{A_2 - A_1}{\Delta t} = \frac{\alpha (A_2 - A_1)}{4} , \tag{3.25}$$

so that

$$\alpha = \frac{4}{\Delta t} . \tag{3.26}$$

For example, if calculation resolution is 1 ms, the fastest transition takes place in 1 ms. Thus, Δt=1 ms and α=4000. This shows that large α is always used, which in turn shows that the approximations in equation 3.23 are correct. The choice of Δt=1 ms is also supported by the auditory nerve fibre decay time constant data discussed after equation 3.7.

Using equation 3.26 in equation 3.23, it is found that

$$var(\hat{\tau}) = \frac{3\Delta t}{4} \cdot \frac{\lambda_1 + \lambda_2}{(\lambda_2 - \lambda_1)^2} \cdot \frac{1}{M}. \tag{3.27}$$

If, in equation 3.21, the transition takes place in one sampling period, then T=Δt, so that the variance in the estimate of τ predicted by equation 3.27 is 1.5 times the variance predicted by equation 3.11. However, it is merely the nature of the transition model (ramp in equation 3.19 or sigmoidal in equation 3.7) which results in this difference. The sigmoidal function with slope as calculated in equation 3.26 does not quite complete a transition within one sampling period. When α= 6/Δt, the transition is completed within one sampling period. With this α in equation 3.23, it is seen that equation 3.21 equals equation 3.23. Thus the estimate is efficient and the variance in estimate is given by the simplified version of equation 3.21,

$$var(\hat{\tau}) = \frac{\Delta t \cdot (\lambda_1 + \lambda_2)}{2(\lambda_2 - \lambda_1)^2} \cdot \frac{1}{M}. \tag{3.28}$$

Equation 3.28 is a simple closed form expression for the variance in the estimate of the change point. This equation can be used to predict the standard deviation in the estimate of the time of transition from an average rate λ_1 to a new average rate λ_2 in a Poisson process, as a function of $\Delta\lambda$, the difference between the two rates.

2.4 Bounds on the gap detection and discrimination thresholds as a function of ΔF

For the gap detection or gap discrimination problem, the variance in the estimate of the time of transition is required as a function of ΔF, the difference in frequency between the two markers that mark the gap. As it is known from the derivations above how $\Delta\lambda$ influences the accuracy with which a change-point can be located, a relation between ΔF and $\Delta\lambda$ is required.

It is assumed that the auditory system places a filter halfway between the two marker frequencies F_1 and F_2. This "filter" is just an "attention window" or observation window and

does not apply any weighting. The width of the window is assumed to be one critical band. When F_1 and F_2 are closely spaced (closer than one critical band), the largest part of the activation pattern of each of the marker frequencies falls within the attention window. A central integration centre that observes inputs from fibres within this observation window will see large differences in firing rate when the fibres are excited by the presence of a marker tone, as opposed to the low firing rate during the gap. Not all the fibres fire at the same rate, of course. The central integration centre will see a firing rate profile. The data of Zhang, Salvi, and Saunders (1990) show that discharge rate may be suppressed below SR during the gap. The rate during the gap is assumed to be SR or lower. The rate profiles for the pre-gap and post-gap markers will be similar, but not equal (figure 3.3). As the marker frequencies are separated (ΔF increases) the observation window will eventually contain just the tails of the

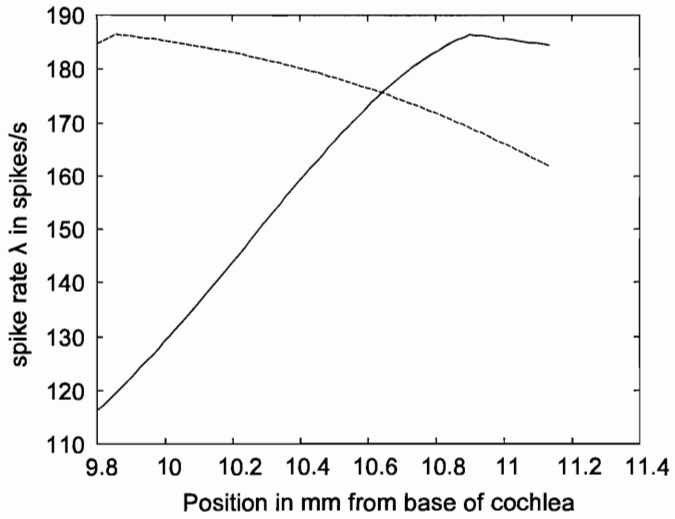

Figure 3.3

Spatial excitation profiles of two marker frequencies are shown when observed in a window one critical band wide (midway between the two sites of maximum excitation). The solid line is for excitation by the first marker of 500 Hz, and the dashed line is for excitation by the second marker of 600 Hz.

activation patterns. Little or no difference in firing rate between the gap and marker conditions exists for this situation, so that the transition between the gap and marker will be difficult to

detect. Using the model in paragraph 2.1 to obtain the firing profile, different values $\lambda_1^{(i)}$ for each fibre in the observation window during the marker is obtained, while it is assumed that a fixed λ_2 exists on all fibres during the gap. λ_1 is the rate during a marker, while the superscript *(i)* indexes the fibre number.

To combine information from the spike trains in the observation window, one option is to calculate the SNR on each fibre and then to add the SNRs (see equation 3.17; Green and Swets, 1966, equation 9.1) to obtain a combined SNR for N channels. This can be substituted into equation 3.20 to obtain a new equation 3.21. Or, to simplify calculations, the maximum λ_1 could be used. This will give the best possible SNR and thus the best possible performance. The effect of N fibres can then be added by multiplying the SNR by N. This method does not take the poorer signal-to-noise ratio on other fibres into account. The first option was used in calculations. This was used in equation 3.21 to calculate the variance in the estimate of τ, the time of the transition between the marker and the gap.

It was further assumed in calculations that the two markers had the same average value of λ_1, and that both transitions (from marker to gap and from gap to marker) were of equal difficulty to estimate. If the noise in measuring the exact time of transitions were the only source of noise in estimating gap length, then the variance in the estimate of the gap length is the sum of the variances of the estimates of the two transition times. Following Siebert (1970), the standard deviation in the estimate of gap duration can be equated to the gap duration discrimination threshold jnd_{gap},

$$jnd_{gap} = \sqrt{2\,var(\hat{\tau})}\,. \qquad (3.29)$$

$Var(\hat{\tau})$ is calculated from equation 3.21. Equation 3.29 is for a single fibre and is valid under the assumption that the two random variables indicating the two transitions on either side of the gap are independent.

Figure 3.4 shows data sets for gap detection (Formby et al., 1996) and gap discrimination

(Divenyi and Danner, 1977) along with predictions obtained from equation 3.29 and other predictions to be described in the sequel.

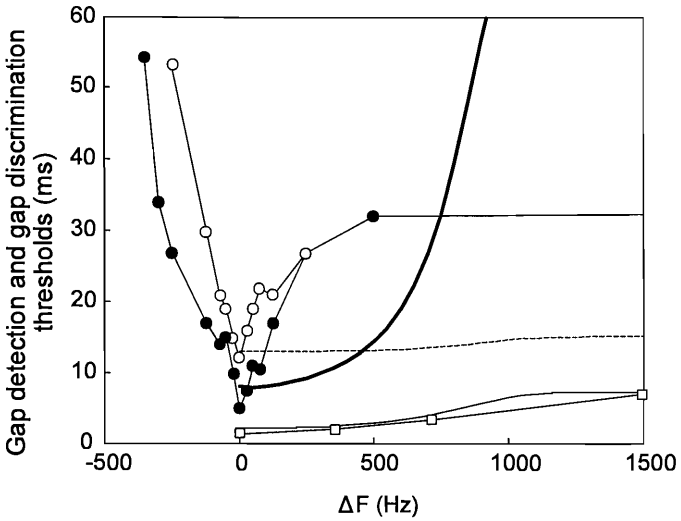

Figure 3.4

Gap detection and discrimination data and model predictions for gap discrimination are shown. Circles are gap detection data from Formby et al. (1996). The standard (first marker) was at 500 Hz in these data. Open circles are for a signal-to-noise ratio of 40 dB with noise presented at 10 dB SL, while closed circles are for the same signal-to-noise ratio, but presented at a louder level (noise at 30 dB SL). Squares are gap discrimination data from Divenyi and Danner (1977). Model predictions have been obtained only for F_2 (post-gap marker frequency) higher than F_1 (pre-gap marker frequency). The thin solid line and dashed line are model predictions for gap discrimination, while the bold solid line is a prediction for gap detection. The dashed line for gap discrimination was obtained when the Poissonian timer was implemented, and the solid line was obtained without the Poissonian timer. Model parameters were: fibre threshold = 45 dB, k=20, σ_0=5, SR=35 spikes/s, maximum spike rate = 200 spikes/s.

2.5 Measurement of gap duration with a Poissonian timer

It is possible that the internal time measurement is also noisy, i.e. when the only source of noise is not only the noisy measurement of gap edges, but also imperfect measurement of the time between the two estimates of gap edges. Creelman (1962) and Divenyi and Danner (1977) addressed the problem of measuring the gap duration with a timing mechanism that measured the gap duration by counting the number of spikes of a Poisson spike train when the gap edge positions are known. In this document, this mechanism of measuring gap duration is referred to as a "Poissonian timer".

With the gap edge positions known, but measurement of gap duration is done with a Poissonian timer, d' is (Divenyi and Danner, 1977)

$$d' = \sqrt{SNR} = \frac{\sqrt{2}(\mu_{t+\Delta t} - \mu_t)}{\sqrt{\sigma^2_{t+\Delta t} + \sigma^2_t}} . \tag{3.30}$$

μ_t is the average number of spikes during a gap with duration t. For a Poisson process, $\mu_t=\lambda.t$, with λ the rate during the gap, $\mu_{t+\Delta t}=\lambda.(t+\Delta t)$, and the spike count variances are $\sigma_t^2=\lambda.t$ and $\sigma_{t+\Delta t}^2=\lambda.(t+\Delta t)$. The jnd for gap duration is Δt.

The average number of spikes during a gap of duration t is still the same when the gap edges cannot be determined accurately, but the variance in the number of spikes increases. If σ_τ^2 is the variance in the estimate of the gap edge time, the additional number of spikes for one uncertain edge is $\sigma_\tau.\lambda$. Thus, the total variance in the spike count when estimating gap duration is

$$var(spike\ count) = 2 \cdot (\sigma_\tau \lambda)^2 + \sigma_t^2 . \tag{3.31}$$

Then, substituting equation 3.31 in equation 3.30, d' for gap duration is

$$d' = \frac{\sqrt{2}(\mu_{t+\Delta t} - \mu_t)}{\sqrt{\sigma^2_{t+\Delta t} + 4\sigma^2_\tau \lambda^2 + \sigma^2_t}}, \tag{3.32}$$

which is an equation also given in Divenyi and Danner (1977).

The gap duration jnd can be solved for from equation 3.32 by setting d'=1 (this is by definition the discrimination threshold; at d'=1 the percentage of correct decisions is 76%). μ_t and σ_t^2 are substituted by $\lambda.t$, and $\mu_{t+\Delta t}$ and $\sigma^2_{t+\Delta t}$ by $\lambda.(t+\Delta t)$ and then equation 3.32 is solved for Δt, where Δt is the jnd in gap duration,

$$\Delta t = \frac{1}{4\lambda} + \frac{1}{4\lambda}\sqrt{1 + 16\lambda t + 32\sigma^2_\tau \lambda^2}. \tag{3.33}$$

The variable t is the base duration for gap discrimination in this equation, and λ is the average spike rate that the Poissonian timer uses to measure the gap duration. By assumption, this rate is different from the spike rate during the gap, but is the spike rate used by a Poissonian timer somewhere in the central auditory system. To use this equation, σ_τ^2 is required. This is the variance in the estimate of the transition from gap to marker as given in equation 3.29. Figure 3.4 shows the effect on gap thresholds of using a Poissonian timer.

2.6 Gap detection

The derivation so far is valid for a gap discrimination task. For gap detection, the task is quite different, and in this section equations are derived for gap detection thresholds.

In the gap detection task, the listener has to detect the presence of a gap, but does not have to estimate the gap duration. If both markers have the same frequency (the within-channel condition), the task is to detect a transition. If the gap markers differ in frequency (the across-channel condition), there will be a transition whether a gap is present or not. To detect the gap in a 2IFC paradigm, the listener will have to decide which interval has two transitions. Accordingly, two transitions must be detected. The detection of a transition depends on both

the rate difference between two Poisson processes (during the gap and markers), and the time that the detector has to observe the Poisson process before and after the transition. If the gap is too brief, the change in spike rate after the first gap edge will not be detected, and neither will the change in spike rate at the end of the gap. Only one transition will be detected if the markers differ in frequency.

In other words, if the gap is too brief, the listener does not discriminate between the Poisson spike rate during the marker and during the gap. If the difference in spike rate is not discriminated, the gap cannot be detected. Therefore, the central detection mechanism has to obtain an estimate of the spike rate.

Spike rate estimates can be obtained by an optimal nonlinear estimator as described in chapter 5, or sub-optimal estimates may be obtained from spike counts. The nonlinear estimator described in chapter 5 uses the spike train as input and estimates the spike rate of that specific spike train. It bases estimates on a prior model of the expected signal. To obtain statistical information (e.g. variance in estimate), Monte Carlo analysis is required.

On the other hand, statistical methods can be used to evaluate the performance of a classical estimator. In this chapter, the central gap detection mechanism is hypothesized to discriminate spike trains based on the sub-optimal statistic of spike counts. If two Poisson processes that differ in rate have to be discriminated based on the number of spikes in an interval T, the signal-to-noise ratio for the discrimination task is (Rieke et al., 1997; see also equation 3.14).

$$SNR = \frac{T \cdot (\Delta\lambda)^2}{\lambda_{avg}} = \frac{2T(\lambda_2 - \lambda_1)^2}{\lambda_1 + \lambda_2}. \tag{3.34}$$

In this equation, λ_{avg} is the average λ and T is the total observation interval of the Poisson process with rate of either λ_1 (during a marker) or λ_2 (during a gap). As the critical interval for discrimination between the two spike rates is the gap (because it is brief), T can be equated to

the gap duration. In other words, the assumption is that if an observation period of T seconds is too brief to discriminate between two rates λ_1 and λ_2, the gap will not be detected. If T is long enough for discrimination of the spike rate during the first marker from the gap spike rate, and also for discrimination of the gap spike rate from the second marker spike rate, the gap will be detected. If it is assumed that both marker stimuli elicit the same spike rate, and that the (lower) spike rate during the gap is stationary, detection of both transitions are equally likely.

The threshold value for the detection of the gap is where P_d=P(gap detected)=0.76 (i.e., when d'=1 in a 2IFC paradigm). For the detection of a gap,

$$P(\textit{gap detect}) = P(\textit{detect first transition}) \cdot P(\textit{detect second transition}) . \qquad (3.35)$$

For achieving a detection probability of P_d=0.76, the probability of detection for either transition has to be 0.87 ($0.87^2 = 0.76$), if it is assumed that the detection of both markers is equally likely.

The detectability d' required for P=0.87 is then calculated from

$$P(\textit{detection of transition}) = 1 - Erfc\left(\frac{\sqrt{2}\ d'}{2}\right) = 0.87 , \qquad (3.36)$$

which is valid for a 2IFC experimental paradigm.

For P=0.87, it is found that d'≈1.6. This value for d' is substituted into equation 3.34, keeping in mind that d' = $\sqrt{}$SNR. Solving for T,

$$T = \frac{1.6^2\ (\lambda_1 + \lambda_2)}{2(\lambda_2 - \lambda_1)^2} . \qquad (3.37)$$

This is the final equation for the gap detection threshold, where T is the gap duration, and λ_1 and λ_2 are the spike rates during the marker and gap respectively. For comparison with the gap discrimination threshold, equation 3.22 is repeated here,

$$std\ dev(\tau) = \sqrt{\frac{\Delta t^2(\lambda_1 + \lambda_2)}{2T(\lambda_2 - \lambda_1)^2} \cdot \frac{1}{M}}. \qquad (3.22)$$

Note that in equation 3.37 the quantity $(\lambda_1 + \lambda_2)/2(\lambda_2 - \lambda_1)^2$ appears, while the square root of this same quantity appears in equation 3.22. This characterizes the difference between gap detection and discrimination. This is equivalent to the situation of intensity discrimination, where it is well known that for detection, data can be fit by a normal integral of A^2 (where A is the stimulus intensity), while for discrimination the data is fit by a normal integral of ΔA (e.g., Laming (1986)).

As before, values of $\Delta\lambda$ correspond to a particular ΔF, so that curves for the gap detection threshold as a function of ΔF can be plotted. Examples of gap detection threshold predictions are shown in figures 3.4-3.7 (discussed below).

3 RESULTS

Figures 3.4-3.7 show gap detection data (Formby, Sherlock, and Forrest, 1996) and gap discrimination data (Divenyi and Danner, 1977) for acoustic stimulation and listeners with normal hearing, along with model predictions. The Formby data were measured for F_1=500 Hz and a variable F_2. Two data sets are shown, both measured at a SNR of 40 dB, but the data set with the lower gap threshold was measured at higher intensity (the noise level was 30 dB SPL instead of 10 dB SPL). The data show that discrimination of gap duration is an easier task than gap detection under the conditions of these experiments (where noise complicated the gap detection task). Possibly, the presence of the base duration makes this task simpler than gap detection.

Model predictions for various parameter choices are shown in figures 3.4 to 3.7. Model parameters are described in the figure captions. Three model curves are shown in each figure, one for gap detection thresholds (equation 3.37), one for gap duration discrimination when the

only source of noise is the uncertainty in gap edge positions (equation 3.22), and one for gap duration discrimination when the gap duration is measured with a Poissonian timer (equation 3.33 together with equation 3.21).

Overall, the trends shown by the gap detection model and the gap duration discrimination model parallel those observed in the data. The gap detection curves have steeper slopes than the gap duration discrimination curves. The latter curves are wide, bowl-shaped curves. However, the predicted gap detection thresholds are lower than the gap discrimination threshold for within-channel gap detection ($\Delta F=0$) when the Poissonian timer is used.

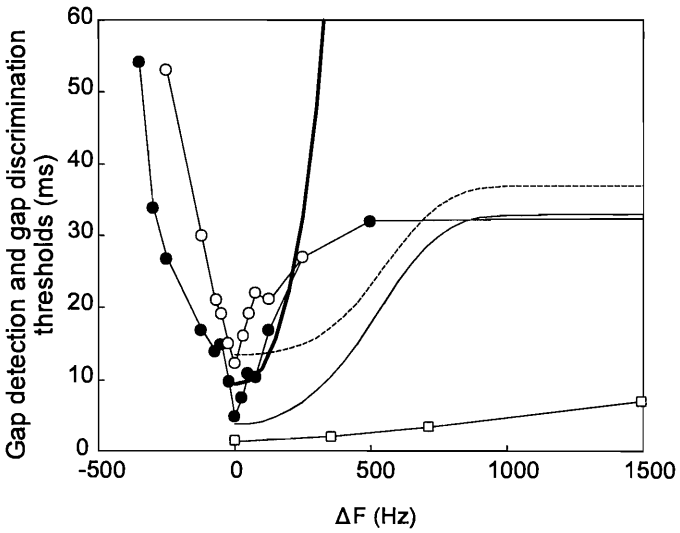

Figure 3.5

Same as figure 3.4, but with different model parameters: fibre threshold = 55 dB, k=20, σ_0=5, SR=25 spikes/s, maximum spike rate = 200 spikes/s. The thin solid line and dashed line are model predictions for gap discrimination, while the bold solid line is a prediction for gap detection.

For the parameter choices in figure 3.5, the tip region of the gap detection data is predicted by the gap detection model, while the tails of the gap detection data are predicted by the gap discrimination model. However, neither model predicts the gap discrimination data. Note that for both the gap detection and gap discrimination models, the same fibre parameters were used. It is, however, conceivable that gap detection and gap discrimination are performed by fibres

with different parameters.

The model predictions in figure 3.6 are interesting. For these parameter values, the gap detection model predicts the gap detection data, while the gap discrimination model with the same parameters predicts gap duration discrimination thresholds in the correct range, although the wide-bowl shaped curve is not predicted. Considering the gap discrimination model where the Poissonian timer is used, it is observed that the sharp peak in the electrical stimulation data (see figures 2.2, 2.3 and 2.12) is predicted by the gap detection model, while the wide bowl-shaped part of the electrical stimulation data is predicted by the gap discrimination model. There is a change-over point at a gap duration of 13 ms, so it seems possible that at this duration the task changes from detection to discrimination. This is at a value of ΔF of 100 to 150 Hz, which is approximately one critical band at a marker frequency of 500 Hz. Interestingly, this is supported by pitch discrimination data for electrical stimulation (Hanekom and Shannon ,1996), where electrode sounds generally become distinct when electrode pairs are 1.5 mm apart (approximately one critical band).

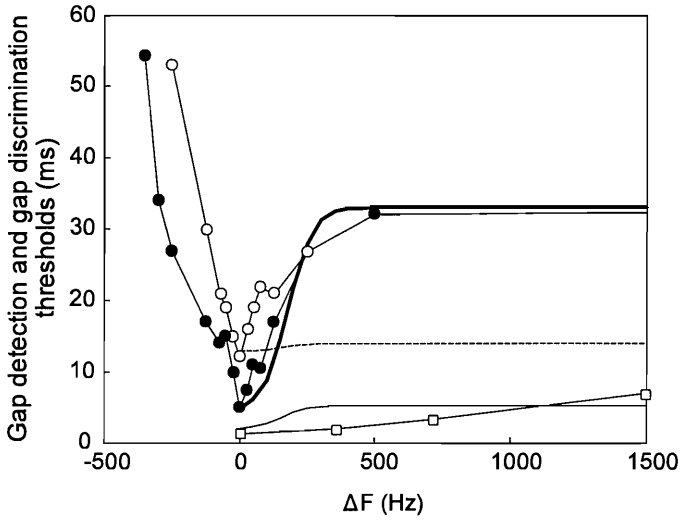

Figure 3.6

Same as figure 3.4, but with different model parameters: fibre threshold = 55 dB, k=20, σ_0=2, SR=35 spikes/s, maximum spike rate = 200 spikes/s.

If the resolution is 1 ms, and if α is chosen as $4/\Delta t$, then α=4000. With this choice and with fibre threshold set at 45 dB in the gap discrimination model, it is seen in figure 3.4 that a

reasonable fit is obtained to the gap discrimination data. This suggests the possibility that the gap detection thresholds and gap discrimination thresholds are not determined by the same population of nerve fibres. For these parameter choices, it is also observed that only one fibre is required to achieve the gap discrimination data if gap duration measurement is perfect, but if the measurement is done with a Poissonian timer, more fibres are required. Other parameter choices also need to be changed to predict the data in this case. Specifically, the base duration for discrimination has to be 0 to achieve low enough gap discrimination values with the Poissonian timer. Equation 3.33 shows that gap thresholds may be decreased by decreasing the base duration, or by increasing λ, the rate of the Poissonian timer.

In some of these simulations, the neural threshold was set at 55 dB. This is an unrealistic choice. This value is required to achieve a sharper cutoff in λ_2 (i.e. a narrower region of activation). This means that after the auditory nerve, an additional system must exist which sharpens neural tuning, or, equivalently, inhibits neural firing when the frequency difference between CF and the stimulus frequency is large enough.

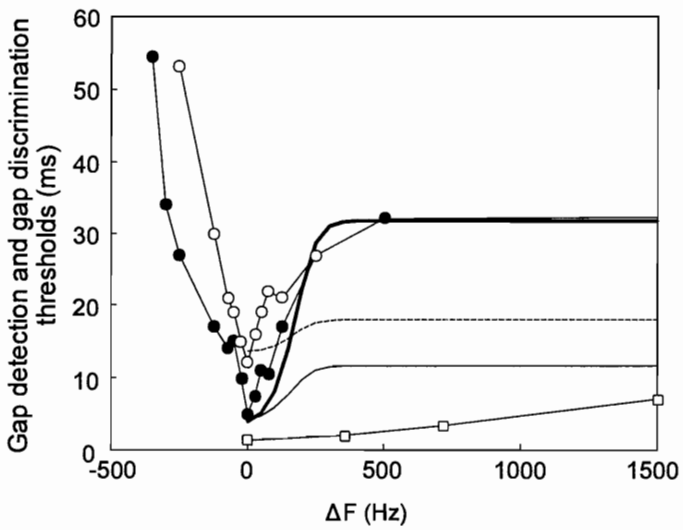

Figure 3.7

Same as figure 3.4, but with different model parameters: α_0=12, fibre threshold = 35 dB, k=20, σ_0=7, SR=40 spikes/s, maximum spike rate = 200 spikes/s.

Apart from the unrealistically high value of threshold, another parameter controls the roll-off

rate of λ_2. This is the tuning parameter α in equation 3.5, which controls the sharpness of tuning. With α_0=4 in equation 3.6, the model tuning curves provide good approximations to the data of Kiang et al. (1965). This is at the auditory nerve level. With α_0=12, tuning is much sharper, but compares with the tuning found at higher levels of the central auditory nervous system.

Cells in the DCN (dorsal cochlear nucleus) are known to exhibit sharp cutoff and inhibitory areas. Cells have also been found in the DCN that have extremely sharp roll-off (Rhode and Greenberg, 1992). Also, frequency tuning in the central auditory system improves deeper into the auditory system. Tuning is sharper at the auditory cortex than at the CN level, which in turn has sharper tuning than the auditory nerve (Sutter, 2000). Sutter gives examples of cells in A1 that have much sharper tuning than what is required to fit the gap detection data. It is quite possible that gap detection takes place at the CN level but the goal here is not to prove or disprove this.

Using this sharper tuning (α_0=12 in equation 3.6), and other more realistic parameter choices, it is shown in figure 3.7 that the gap detection data are approximated quite well by the model. The parameters are shown in the figure caption. Note that the sharp curve is still obtained for high threshold fibres only, but now the model fibre threshold is more realistic. For low threshold fibres, the model predicts better performance. Thus, it seems the auditory system does not perform optimally in this task.

4 DISCUSSION

4.1 Strengths and shortcomings of the model

The expressions that were derived for gap detection and discrimination thresholds as a function of the spike rates during the gap and markers, seem intuitively correct. Building on these, the model provides closed form expressions for gap detection and discrimination thresholds. It is

seen that the model can predict both the magnitude and the trends in the gap detection and gap discrimination data for certain choices of model parameters. The sharper curves for gap detection and the shallower curves for gap discrimination are predicted.

The model assumes that the gap detection mechanism uses sub-optimal statistics (spike counts) in a classical detector to detect the presence of a gap. No prior knowledge of the signal dynamics is used (as opposed to the model of chapter 5). However, as argued in chapter 5, it is likely that the auditory system uses an internal model of the spike generation mechanism.

The models for gap detection and discrimination do not provide an explicit mechanism that can detect a gap from a spike train input. Therefore, it is perhaps not immediately evident that the model for gap discrimination implicitly assumes that λ_1, λ_2 and λ_3 are known, i.e. the calculated CRLB for position of the gap edge assumes that the spike rate during the gap and markers are known. This is not an unreasonable restriction, as it is possible that the auditory system estimates spike rates. Regardless, the CRLB gives a lower bound on the accuracy of the estimation of gap edge times, and possibly the auditory system does not achieve this lower bound. This is supported by gap detection and discrimination data.

To use classical signal detection theory to predict gap thresholds, meant that a simple signal model (spike train model) was required. Closed form expressions could be obtained because spike trains were assumed to be Poissonian. The Poissonian assumption is usually only valid at higher frequencies or deeper in the central auditory nervous system where no phase-locking occurs. However, as argued in the introduction, it is reasonable to use Poissonian spike trains in a model for gap detection, as it seems that temporal information does not play a significant role in determining across-channel gap detection thresholds. Chapter 4 discusses the gap detection problem when phase-locking occurs.

4.2 Parameter sensitivity and the origin of the shape of the gap detection tuning curves

The predicted magnitude of gap detection thresholds by equation 3.37 is consistent with data when realistic values for λ_1 and λ_2 are used. The shapes of the gap detection tuning curves are

determined by several model parameters.

The sharp tips of the gap tuning curves are controlled primarily by the roll-off of the λ versus ΔF function. The sharper the slope of this function, the sharper the tip of the gap detection tuning curve. The slope of this function is, in turn, controlled by α_0 in equation 3.6, which determines the sharpness of tuning.

The slopes of the tuning curve flanks are controlled by σ_0, which determines the slope of the rate-intensity curve. Larger σ_0 result in shallower rate-intensity curves and shallower tuning curve slopes.

The flattening of the gap detection tuning curve beyond the shoulder of the curve is obtained when the spike rate during a gap is less than the SR. The spike rate during the gap may be less than SR when suppression of spike rate occurs after the offset of the first marker (Zhang et al., 1990). The flattening of the tuning curve occurs because, for widely spaced marker electrodes (large ΔF) the spike rate in the observation window during a marker reaches a steady state value (the spontaneous rate SR). As the spike rate during the gap is also fixed in the model, it is seen from equation 3.37 that gap threshold T will reach a steady state value.

4.3 Temporal and spatial models for gap detection

The model hinges on the idea that the auditory system uses an attention filter or observation window that is placed midway between the regions excited by the two markers. As explained in more detail in chapter 4, evidence does exist which challenges this idea. Nonetheless, the model has made concrete the notion that "the task becomes more difficult" as marker frequencies are separated. Increased difficulty of the task is reflected in spike rates during the markers and gap that become more similar as marker frequencies are separated. This is a spatial model for gap detection, as opposed to a temporal model for gap detection. As discussed in the introduction, evidence exists that supports the notion that at least across-channel gap thresholds are based on spatial mechanisms.

Zhang, Salvi, and Saunders (1990) have shown that spike rate decays exponentially after the offset of the first marker, so that the gap is filled with continuing spike activity and therefore brief gaps are difficult to detect. Filling of the gap provides a feasible explanation for within-channel gap detection thresholds, but cannot explain increases in gap thresholds in the across-channel condition.

Whether temporal mechanisms or spatial mechanisms are used to explain gap thresholds, it is clear that separating the marker frequencies results in deteriorated signal-to-noise ratios in the spike train or set of spike trains that the detection mechanism observes. The "signal" that has to be detected in either case is the transition from marker to gap (or gap to marker) that is masked by some source of noise.

4.4 Interpretation of modelling results

To predict gap detection data accurately, especially the sharp tip region, the model requires unrealistically high fibre thresholds when neural tuning curves are modelled after auditory nerve tuning. When sharper tuning is assumed, similar to that found in some DCN fibres or deeper in the central auditory nervous system, the sharp tip region is predicted more easily, but still using high threshold fibres. There is no apparent reason why only high threshold fibres would take part in gap detection.

Assuming more realistic fibre parameters, predicted gap thresholds are smaller than measured gap thresholds in the across-channel condition. The auditory system seems to operate sub-optimally in this task, an observation that has also been made regarding frequency discrimination ability (Siebert, 1970; Hanekom and Krüger, 2001). Spike count statistics are already suboptimal for rate discrimination or transition detection, but even so deterioration of gap detection thresholds in the across-channel condition is faster than the model predicts.

The fact that sharp tuning is required to predict gap detection data with this model suggests that theoretically the auditory system should be able to perform much better on the gap detection task, but is somehow limited by internal noise or other confounding factors. It may

be that subjects find it difficult to attend to the gap because of the different-sounding markers (van Wieringen and Wouters, 1999), but this is probably more important in cochlear implantees than in normal-hearing listeners. The task of detecting a gap between spectrally different sounds occurs frequently in normal hearing, e.g. voice onset time is one feature that distinguishes different consonants.

It is outside the scope of this work to determine where in the auditory system the gap detection mechanism is situated, but it can be speculated on. With many free parameters controlling the shape of the model-predicted gap detection tuning curves, it is important that parameter choices should be biologically plausable. It is therefore adequate to show that the parameter values required to fit the data are in line with neural parameters published in literature. The fact that sharp tuning is required to predict gap detection data points to the possibility that the gap detection mechanism is implemented at the CN level or deeper in the central auditory nervous system.

Finally, comparing model predictions with the data, it seems possible that the task changes from gap detection to gap discrimination at a certain frequency separation (possibly at one critical band, as shown before).

5 CONCLUSIONS

The CRLB for the Poisson change-point problem, which appears not to be documented in literature, has been derived here. The result is intuitively satisfying.

It is shown that the quantity $(\lambda_1 + \lambda_2)/2(\lambda_2 - \lambda_1)^2$ appears in the model for the gap detection task, while the square root of this same quantity appears in the gap discrimination model. A similar observation regarding intensity discrimination has been made before.

A model that can predict the U-shaped curves found in across-channel gap detection has been created. The model is simply based on signal detection theory considerations.

The model shows that a spatial mechanism, as opposed to temporal mechanisms, may contribute to gap detection thresholds in the across-channel condition. This is important in cochlear electrical stimulation, where spike trains are strongly phase-locked to the stimulus and where temporal mechanisms do not seem to determine gap detection thresholds. Accordingly, techniques similar to those used in this chapter are applied in chapter 3 to create a model that can predict gap detection thresholds in auditory electrical stimulation.